Enabling Automation of Friction Stir Welding: The Modulation of Weld Seam Input Energy by Traverse Speed Force Control

William R. Longhurst
e-mail: russ.longhurst@vanderbilt.edu
russlonghurst@comcast.net

Alvin M. Strauss
Professor of Mechanical Engineering
e-mail: al.strauss@vanderbilt.edu

George E. Cook
Associate Dean for Research
and Graduate Studies
e-mail: george.e.cook@vanderbilt.edu

Department of Mechanical Engineering,
Welding Automation Laboratory,
Vanderbilt University,
VU Station B 351592,
2301 Vanderbilt Place,
Nashville, TN 37235-1592

Friction stir welding (FSW) joins materials by plunging a rotating tool into the work piece. The tool consists of a shoulder and a pin that plastically deforms the parent materials and then forges them together under the applied pressure. To create the pressure needed for forging, a rather large axial force must be maintained on the tool. Maintaining this axial force is challenging for robots due to their limited load capacity and compliant nature. To address this problem, force control has been used, and historically, the force has been controlled by adjusting the plunge depth of the tool into the work piece. This paper develops the use of tool traverse speed as the controlling variable instead of plunge depth. To perform this investigation, a FSW force controller was designed and implemented on a retrofitted Milwaukee Model K milling machine. The closed loop proportional, integral plus derivative (PID) control architecture was tuned using the Ziegler–Nichols method. Results show that the control of axial force via traverse speed is feasible and predictable. The resulting system is more robust and stable when compared with a force controller that uses plunge depth as the controlling variable. A standard deviation of 41.5 N was obtained. This variation is much less when compared with a standard deviation of 129.4 N obtained when using plunge depth. Using various combinations of PID control, the system's response to step inputs was analyzed. From this analysis, a feed forward transfer function was modeled that describes the machinery and welding environment. From these results, a technique is presented regarding weld seam input energy modulation as a by product of force control via traverse speed. A relative indication of thermal energy in the welding environment is obtained with the feedback of axial force. It is hypothesized that, while under force control, the controller modulates weld seam input energy according to the control signal. The result is constant thermomechanical conditions in the welding environment. It is concluded that the key enablers for force control are the unidirectional behavior and load dynamics of the traverse motor. Larger bandwidths and more stable weld conditions emerge when using traverse speed instead of plunge depth to control the force. Force control of FSW via traverse speed has importance in creating efficient automatic manufacturing operations. The intelligence of the controller naturally selects the most efficient traverse speed.
[DOI: 10.1115/1.4001795]

1 Introduction

Friction stir welding (FSW) is a solid state joining process that utilizes a rotating nonconsumable tool to plastically deform and forge together parent metals. FSW tools contain two necessary features for the joining process. These features are a shoulder and a pin (or probe). The shoulder is used to generate heat and forging pressure within the localized welding area. The pin, which resides beneath the shoulder, is used to plastically deform the parent metals of the work piece. Plastic deformation takes place as the pin shears off thin layers of material from the parent metals and rotates them to the backside. At the backside of the pin, the pressure from the shoulder consolidates the deformed parent metals.

For the case of butt welding together two plates, the FSW tool is plunged into the work piece at the intersection of the two plates. When fully plunged into the work piece, the pin is completely submerged below the surface, while the shoulder resides at the surface or just below it. During the joining process, the tool traverses along the faying surface with the pin's axis of rotation in the same plane as the faying surface. Once the tool has reached the end of the weld seam, it is extracted. After extraction, a solid joint exists between the two plates. The process is illustrated in Fig. 1.

Since its inception in the early 1990s, FSW has emerged as a viable welding process for many metals. Historically, the process utilizes the control of three process parameters. These parameters are tool plunge depth, traverse, and rotation speed. As FSW technology continued to develop, axial force became an important process variable that needed to be controlled in closed loop architecture. Force control is particularly important for robotic application of FSW because of its compliant nature [2]. Robotic compliance makes the application of FSW very challenging if not impossible without force control. Without a sufficient axial force acting through the tool, the forging of the plastically deformed work piece would not occur. As a robot continually repositions the FSW tool along the weld path, deflection in the robot's linkages and joints would cause undetectable plunge depth variations. FSW tool plunge depth variations lead to axial force variations and typically insufficient forging pressure beneath the shoulder of the tool. Hence, with insufficient forging pressure, severe welding defects and inadequate joining may occur. With nonrobotic applications, an adequate axial force is typically achieved with the com-

Contributed by the Dynamic Systems Division of ASME for publication in the JOURNAL OF DYNAMIC SYSTEMS, MEASUREMENT, AND CONTROL. Manuscript received May 28, 2009; final manuscript received March 28, 2010 published online June 15, 2010. Assoc. Editor: Marcio de Queiroz.

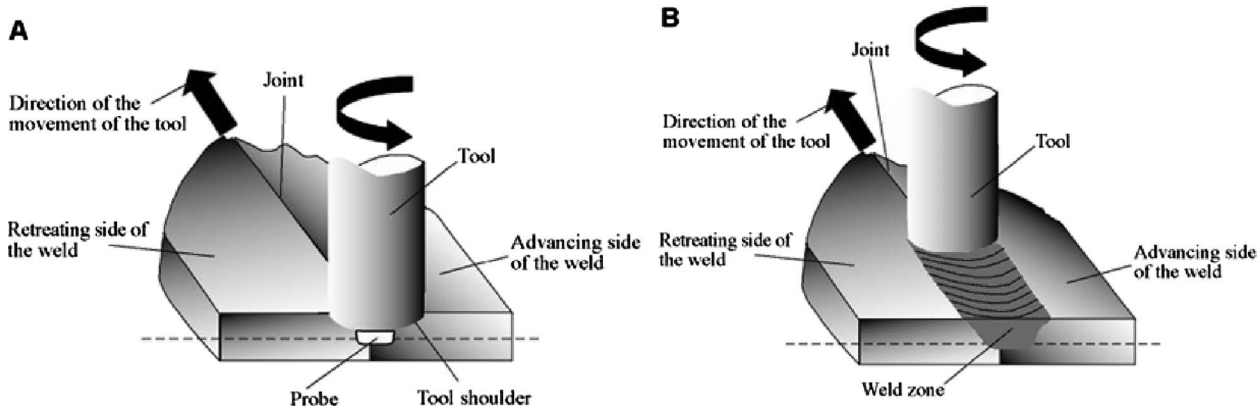

Fig. 1 Illustration of the FSW process [1]

bination of a sufficient plunge depth of the tool into the work piece and the structural rigidity of the applying machine.

Past research at Vanderbilt University by Cook et al. [3] showed the axial force to be a function of tool plunge depth, traverse speed, and rotational speed. Figure 2 illustrates the relation between the axial force and traverse speed. As the traverse speed is increased, the axial force increases as well.

The experimental results show the welding environment to be stiffer for lower tool rotation speeds. This is due to less heat generation and the subsequent reduction in the softening of the work piece material. For a given rotational speed, the axial force changes as a function of traverse speed. The results suggest that large changes in axial force can be obtained by varying the traverse speed. These changes in axial force are greater at slower rotation speeds and less at higher rotation speeds.

Historically, force control of FSW has been accomplished by varying the plunge depth of the tool. Examples are found in the published work by Smith [4], Soron and Kalaykov [5], Zhao et al. [6], Talwar et al. [7], and by Strombeck et al. [8]. Each of these authors developed and implemented a force control architecture using plunge depth as the controlling variable. All were able to conclude that it was feasible to implement FSW force control. However, using plunge depth as the controlling variable presents several challenges. Soron and Kalaykov concluded that even with the implemented action of force control to a robotic FSW system, axial force oscillations will exist when the tool makes contact with the material. They also noted that the penetration depth is hard to predict due to the positioning error of the robot. Zhao et al. presented a nonlinear axial force controller they developed and implemented for a FSW process. They were able to experimentally characterize the static and dynamic behavior of the interaction between the FSW tool and the work piece. With this information and using an open architecture control system, they were able to design a controller using polynomial pole placement. Good results were obtained, but to handle the nonlinear transient response when the plunge depth of the tool changed, the control system had to incorporate experimentally obtained dynamic parameters. Thus, the open architecture of the control platform was needed in order to implement this force controller, and the controller parameters were specific to their experimental setup. Smith was able to use actuator torques as a measurement of the FSW force through the Jacobian relationship [9]. He found the process to be limited to due the necessary update time needed to calculate the axial force. Strombeck et al. used a parallel robot to perform force controlled FSW, but its design was more constricted as compared with an articulating arm robot. Talwar et al. used an elec-

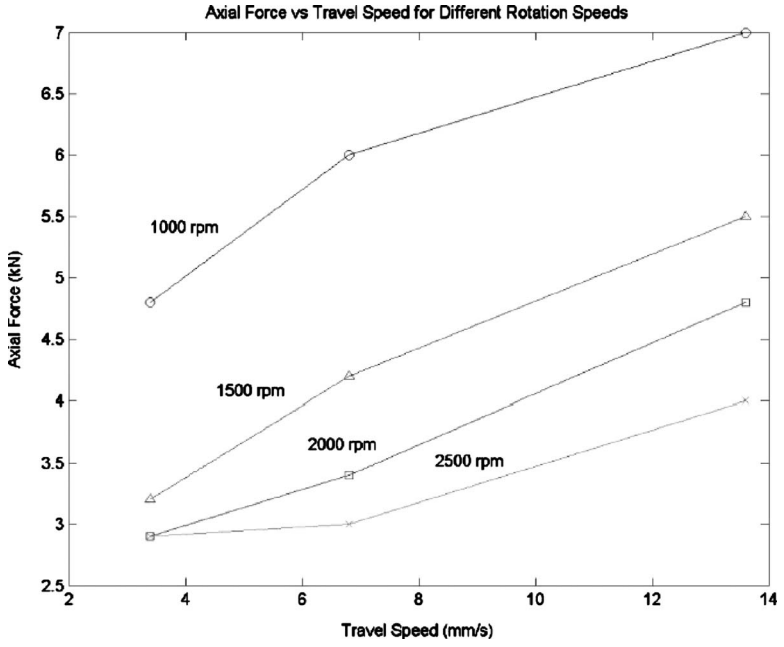

Fig. 2 Axial force as a function of traverse speed [3]

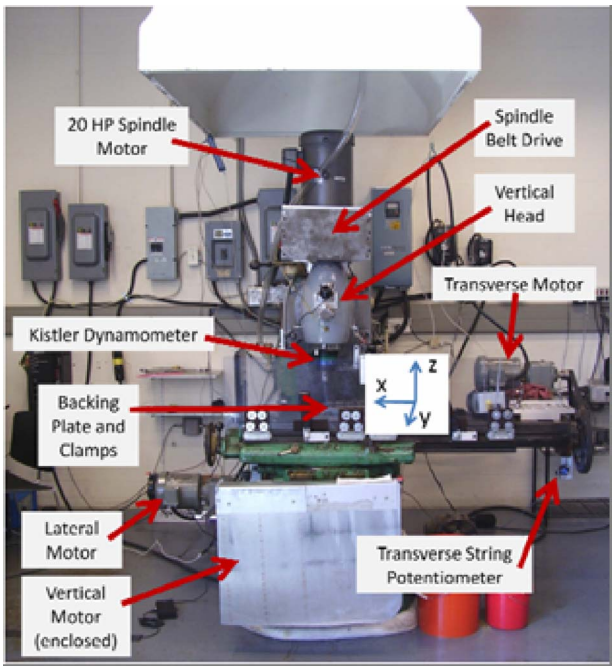

Fig. 3 FSW machine at Vanderbilt University

tromechanical force actuator on a five-axis mill. Talwar et al. found it essential to use axial force control to produce lap welds.

To the authors' knowledge, there has not been any published research on the force control of FSW using the traverse speed of the tool as the controlling variable. The goal of this research is to create a FSW force control architecture that utilizes traverse speed as the controlling variable, and to investigate the resulting force controlled environment. Since the controlling variable is traverse speed, the plunge depth of the tool remains constant.

Presented in this research is the experimental force control architecture. From this experimental architecture, the controlled response of the system is characterized and the contributing elements to the response are identified. Comparisons are drawn between the performance of this experimental FSW force control system that utilizes traverse rate, and a FSW force control system that utilizes the plunge depth as the controlling variable. It is concluded that this control strategy provides a very robust and stable architecture for force control. Lastly, a hypothesis is presented along with supporting evidence that weld seam energy is modulated as a byproduct of force control via traverse speed. The modulation of weld seam energy produces constant thermomechanical conditions in the welding environment.

2 Experimental Configuration

The experiments were conducted on the FSW system at Vanderbilt University. The FSW system is a Milwaukee Model K milling machine that has been retrofitted with more advanced motors and instrumentation. The system is shown in Fig. 3. These retrofits were previously added to automate the system and provide a programmable platform for FSW experimentation. At the top of the control hierarchy is a master computer that enables all of the systems subcomponents such as the motor drive controllers and instrumentation. The master computer is a Dell Precision 340 that uses Microsoft Windows XP as its operating system. The welding and force control code was written in C#. A graphical user interface within the C# software allows the operator to select the desired welding parameters for the pending operation. These parameters include the rotation speed, traverse speed, plunge depth, and weld path position of the tool.

The traverse axis coincides with the milling machine worktable's cross axis. The worktable resides in its saddle by sliding dovetail joints and is driven by a power screw. The power screw is rotated via a system that consists of a belt and pulley attached to the shaft of the power screw. A 1 hp (745.70 W), 6.02 reduction Syncrogear gear motor is attached to the drive pulley. The gear motor is controlled by a Cutler–Hammer MVX9000 Sensorless Vector variable frequency drive (VFD). Command signals are sent directly from the master computer to the VFD. The traverse position is obtained from a string potentiometer. Analog position data from the potentiometer is fed into a sensor box where it is converted to a digital signal, prior to being sent to the master computer.

Welding force data is collected through a Kistler rotating cutting force dynamometer. The dynamometer collects x-axis force, y-axis force, z-axis force, and the torque about the z-axis. The analog signal from the dynamometer is sent to a signal conditioning box where it is converted from an analog signal to a digital signal. Once converted, the data is sent to a separate computer where the data is sorted, recorded, and displayed before being sent to the master computer.

An overview of the closed loop force control system is illustrated by the control diagram of Fig. 4. Within the master computer, a desired z force is selected. The desired force value is subtracted from the actual z force value to obtain a force error.

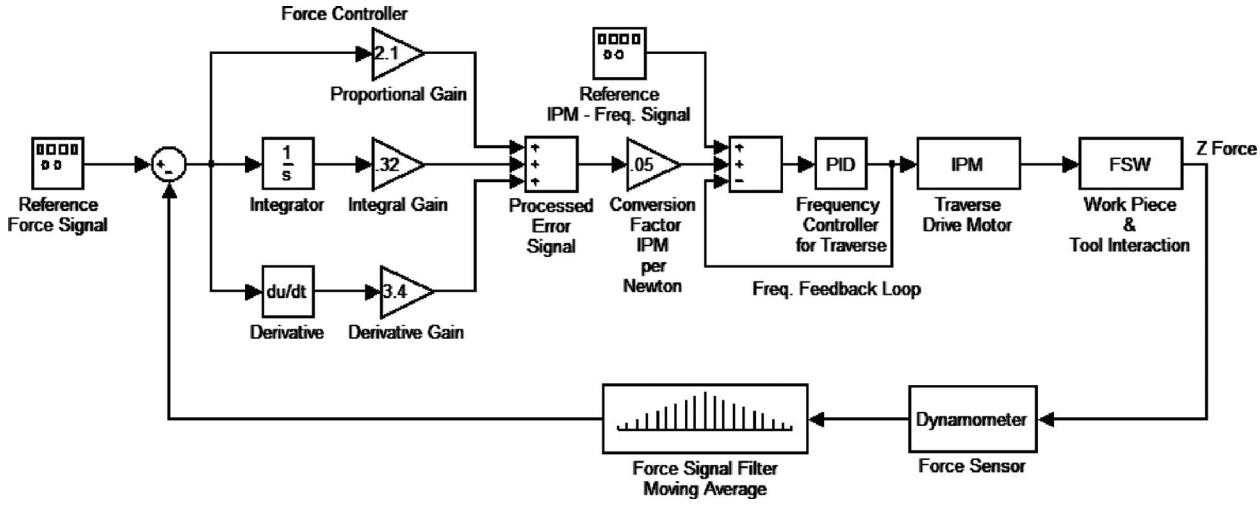

Fig. 4 Control diagram of force control via traverse speed

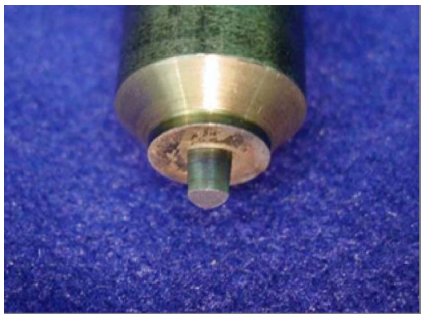

Fig. 5 Trivex pin tool

Fig. 6 Treaded pin tool

The force error signal is then processed in the control law. The resulting processed control signal is then multiplied by a factor of 0.05 to translate the signal from Newtons of force to desired inches per minute of traverse speed. The desired inches per minute is converted to the corresponding frequency and then sent to the VFD. The VFD produces the desired change in traverse speed to obtain the desired value of z force in the welding environment. The dynamometer reads the resulting force and returns it to the master computer where it is once again compared with the reference signal.

The measured z force signal was very noisy. This noise makes the process of applying derivative control to the system very difficult. The noise would simply be amplified by the controller. To address this problem, a filter was implemented. The filter is a five point moving average of the z force with an interrupt frequency of 3.33 Hz. For this experimental setup, these filter parameters were found to provide adequate noise reduction without adding too much phase lag in the signal.

The control law consisted of proportional, integral plus derivative (PID) control. To address the transport delay between the initiation of the control signal and the change in force, a simple delay of 1 s in the control update time was utilized. The 1 s delay allowed the FSW tool to change speed and a change in z force to occur.

To tune the PID force controller and achieve optimum control, the Ziegler–Nichols tuning process was used [10]. The Ziegler–Nichols tuning process called for the controller to use only proportional gain while welding. While using proportion control only, a critical gain value was experimentally determined through trial and error. Over the course of several welds, the gain was steadily increased until the resulting z force achieved sustained oscillation. The sustained oscillation constituted a marginally stable behavior. The resulting control gain and time period between oscillations was recorded and used to calculate PID gains for the controller. The resulting PID control law is shown in Eq. (1). In Eq. (1), K_p is the proportional gain, K_i is the integral gain, K_d is the derivative gain, e is the error as a function of time t and u is the resulting control signal as a function of time t

$$K_p e(t) + K_i \int e(t) + K_d e'(t) = u(t) \tag{1}$$

For this force control research, experiments using two different FSW tools were performed. The two tools with their contrasting size and geometry provided insight into the dynamics of the FSW system. The first tool consisted of a slightly undersized 1/4 in. (6.35 mm) Trivex pin with a flat 5/8 in. (15.875 mm) diameter shoulder. The Trivex pin tool is shown in Fig. 5. The second tool consisted of a 1/4 in. (6.25 mm) threaded pin. The threaded pin was 0.235 in. (5.969 mm) long with a diameter of 0.250 in. (6.35 mm) across its threads. The treaded pin tool is shown in Fig. 6. The critical gains, periods, and resulting control gains for each tool are shown in Table 1.

For the experiment, 1/4 in. (6.35 mm) butt welding with full penetration was performed. The material used was aluminum 6061. The work piece consisted of two 1/4 in. (6.35 mm) by 1.5 in. (38.1 mm) by 8 in. (203.2 mm) long samples. Each weld began with the tool plunging into the metal, 1 in. (25.4 mm) from the end of the work piece. Once the tool achieved the desired plunge depth, it dwelled at that location for 5 s in order to soften the work piece by generating additional heat. After dwelling, the tool began to traverse forward at 4 inches per minute (IPM) (101.6 mm per minute). After traversing 1 in. (25.4 mm), the force controller was engaged. The force controller operated in a regulation mode, meaning that whatever the z force was at the time of engagement, it was the selected desired force. The system operated under force control mode until it reached 1 in. (25.4 mm) from the end of the 8 in. (203.2 mm) work piece. Thus, 5 in. (127.0 mm) of welding was conducted for each run under force control. For many of the welds, a step input in desired force occurred after 2 in. (50.8 mm) of regulation. Each step input was 700 N in magnitude. For every weld made, the shoulder of the tool was plunged 0.001 in. (0.0254 mm) below the surface, and the rotation rate of the tool was maintained at a constant 1400 rpm. Prior to engaging the force control, the traverse speed was 4 IPM (101.6 mm per minute).

To provide a base line of the welding environment, a weld was made without any force control using the 1/4 in. (6.35 mm) Trivex tool traveling at 6 IPM (152.4 mm per minute). The results are shown in Fig. 7. The resulting force during the initial tool plunge into the work piece is identified on the figure as the pin plunge and shoulder plunge regions. After the tool has plunged into the work piece and dwelled for 5 s, the forward motion of the tool begins. This point is easily identified as the sharp increase in force after the shoulder plunge and dwell period. After 1 in. (25.4 mm) of forward travel, the force controller is normally engaged at this point. However, for this base line sample, the force controller is not engaged, but the force occurring at the engagement point is

Table 1 Traverse mode force control gains

	K_p	K_i	K_d
	1/4″ Trivex tool Traverse mode: $K\alpha$=3.5, $P\alpha$=13		
PID	2.1	0.3231	3.4125
P	1.75		
PI	1.575	0.1454	
PD	1.575		1.537
	1/4″ Threaded tool Traverse mode: $K\alpha$=4.15, $P\alpha$=7.5		
PID	2.49	0.664	2.3341
P	2.075		
PI	1.8675	0.2873	
PD	1.8675		1.01

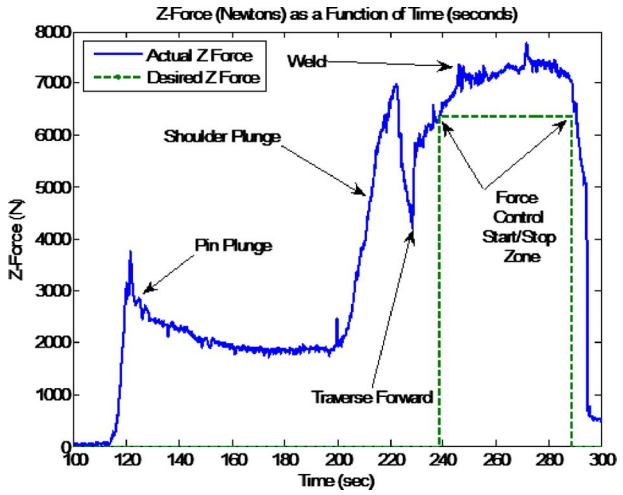

Fig. 7 Weld sample with no force control

displayed as a desired force reference. From the base line sample, it can clearly be seen that the z force continues to increase about two-thirds of the distance across the weld seam. The increase in force is due to the tool moving into the unwelded and colder, less stiff material, as well as thermal expansion of the tool and work piece. The total thermal expansion was calculated to be less than 0.002 in. (0.05 mm), based upon a measured increase of 34°C in the tool as it moved across the work piece.

It can be concluded that the welding process never truly reaches a steady state condition for this particular setup. These transient conditions will provide a good environment to observe the response of the force controller. The system will encounter disturbances that will produce an ever changing error signal for the controller to process and respond to.

3 Results and Discussion

3.1 Force Response. To better understand the value of force control, a welded sample is shown in Fig. 8, where a welding flaw is present due to the lack of force control. The area of the flaw is just past the initial plunge point of the tool. While the 1/4 in. threaded pin tool was in the area of the flaw, the force controller was not yet engaged. However, after traversing 1 in. (25.4 mm), the force controller was engaged and a desired force was selected that eliminated the welding flaw.

A good weld sample created with force control and using the Trivex pin tool is shown in Fig. 9. Its corresponding data is shown in Fig. 10. The results shown in Fig. 10 illustrate the system's ability to regulate the z force. Along with the resulting force, the commanded tool speed is plotted below the force.

As the tool traverses along the weld seam, it slowly decreases speed from 4 IPM (101.6 mm per minute) to approximately 2 IPM (50.8 mm per minute) before gaining speed as it approaches the end of the weld cycle. The tool slows down to reduce the z force.

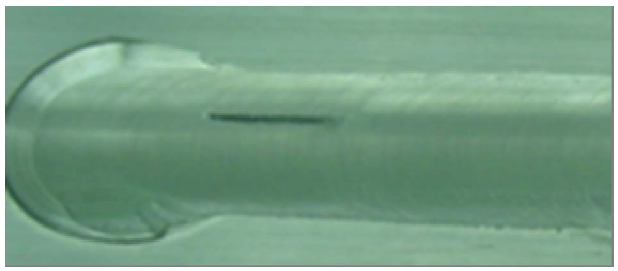

Fig. 8 Weld flaw due to lack of force control

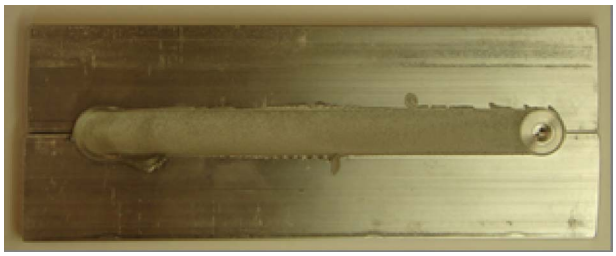

Fig. 9 Weld sample using force control via traverse speed

As the tool is traversing forward, it encounters force disturbances. Since the work piece is positioned on a flat surface, the disturbances are mainly of a thermal nature. Referring back to Fig. 7, which represents a base line welding condition, the z force increases as the tool begins to traverse along the weld seam and across the work piece. This increase in force is due to the tool moving into a colder region, and thus, a stiffer work piece environment than what was previously beneath the tool. When this occurs, the force controller compensates by reducing the traverse speed. As the tool slows down, it allows for more heat to be applied in the localized region underneath the tool. With the additional heat, a softer work piece environment results, which leads to a reduction in the z force.

As the tool nears the end of the work piece, it speeds up. The increase in speed is due to the controller reacting to a softer work piece environment and the need to raise the z force to the desired level established at the beginning of the weld cycle. Over the course of the weld cycle, heat was continually added to the work piece, which softened the work piece.

Analysis of the data presented in Fig. 10 indicates that the force controller performed quite well when compared with other systems that utilize plunge depth as the controlling variable. At the time the force controller was engaged, the desired force was set to 5056 N. Statistical analysis of the collected data revealed that the force controller maintained a mean force of 5053 N. The maximum and minimum values were 5182 N and 4972 N, respectively, with a range of 210 N. Lastly, the standard deviation was determined to be 41.5 N.

As a comparison to the force control with plunge depth as the controlling variable, much greater precision can be obtained when the traverse speed is used as the controlling variable. In separate experiments on the same FSW equipment at Vanderbilt University, force control with plunge depth as the controlling variable

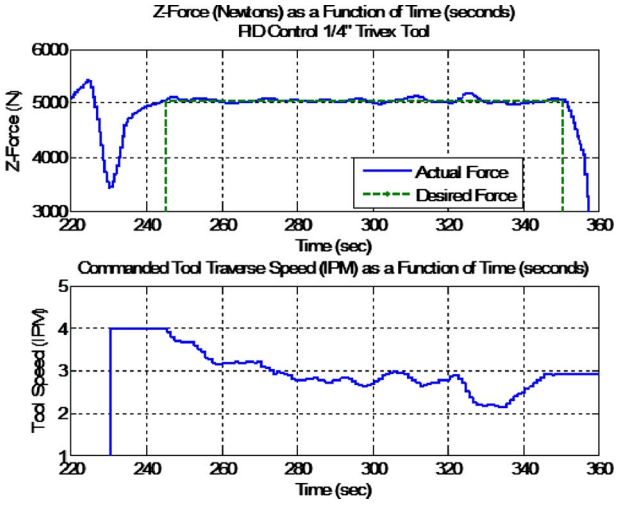

Fig. 10 Regulation of *z* force using force control via traverse speed

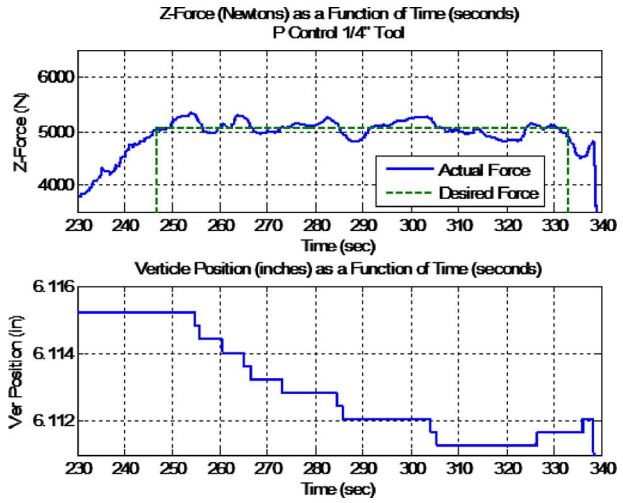

Fig. 11 Force control response when the controlling variable is plunge depth

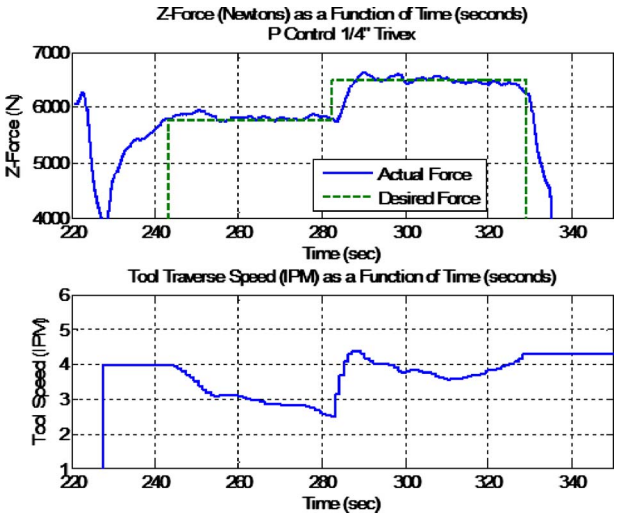

Fig. 13 Regulation and step input with P control

produced results with a standard deviation of 129.4 N when butt welding 1/4 in. (6.35 mm) thick aluminum. Figure 11 shows a response with the corresponding plunge depth data. When using plunge depth as the controlling variable, more force variation exists in the system. Each time the tool is moved either up or down a relatively small amount, a rather larger transient response occurs. This rather large and quick response can become a stability issue for the controller. However, with traverse speed as the controlling variable, the force variation is much less, and the transient response when the tool speed changes, is much smother and controllable as compared with the response when the plunge depth is changed.

As another comparison, Soron and Kalaykov [5] published results for straight line butt welding of 3 mm thick aluminum plates. With plunge depth as the controlling variable, they were able to regulate to a desired z force with a standard deviation of 152 N.

Figure 12 shows the response of the system to a step input of 700 N. The controller was utilizing PID control. After the controller had regulated the force for 2 in. (50.8 mm) of travel, the step was introduced.

The system under PID control responded appropriately to the step input. This is evident by the relatively large overshoot in force. The integrator sums the error and applies the value to the control law, thus contributing to the overshoot. However, it can be noted that the system under PID control did not oscillate. This can be attributed to the derivative term in the controller anticipating the dynamics and reacting before the overshoot occurs to dampen the oscillation. Between the integral and derivative terms, the system behaved in a very robust and stable manner. Other tests with larger step sizes produced repeatable and similar results. The integral term performed as would be expected by eliminating any steady state error. As previously mentioned, the system is subjected to force disturbances as the tool traverses across the system. The force naturally increases as the tool begins to move forward. Without the integrator in the controller, this could lead to a prolonged error. As soon as the force started to increase near the beginning of the weld, the controller quickly compensated due to the integral action.

To gain a better understanding of the unknown dynamics of the system, variations of PID control were implemented. The system responded distinctively to each variation in the control law. These responses can be used in an algebraic manner to determine a transfer function that models the FSW equipment and process.

The responses to the various forms of PID control are shown in Figs. 13–15. The various forms are proportional (P) control, proportional plus integral (PI) control, and proportional plus derivative (PD) control. As would be expected, the performance of the

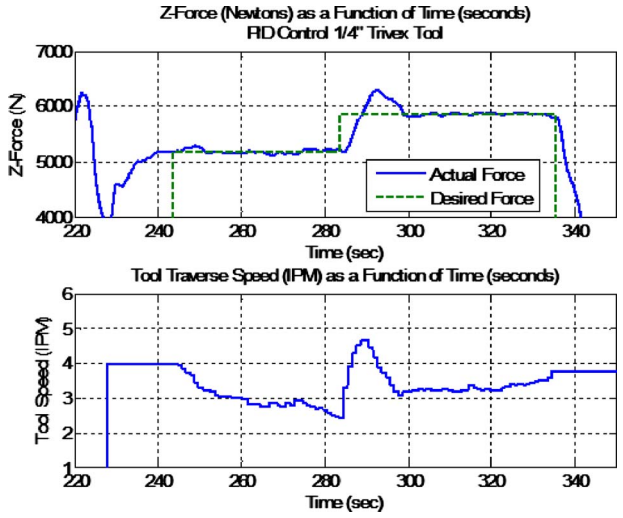

Fig. 12 Regulation and step input with PID control

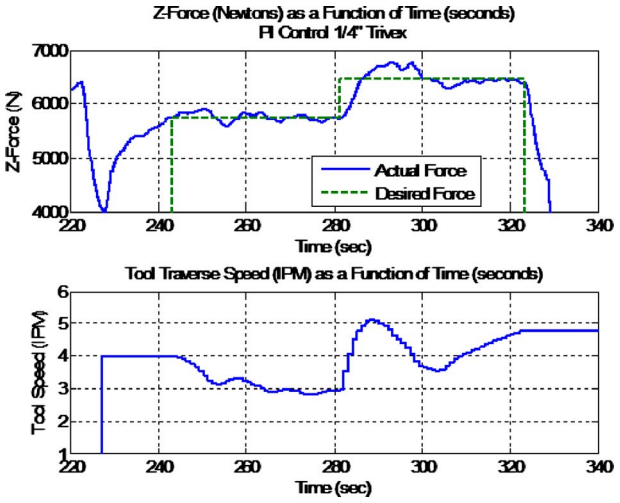

Fig. 14 Regulation and step input with PI control

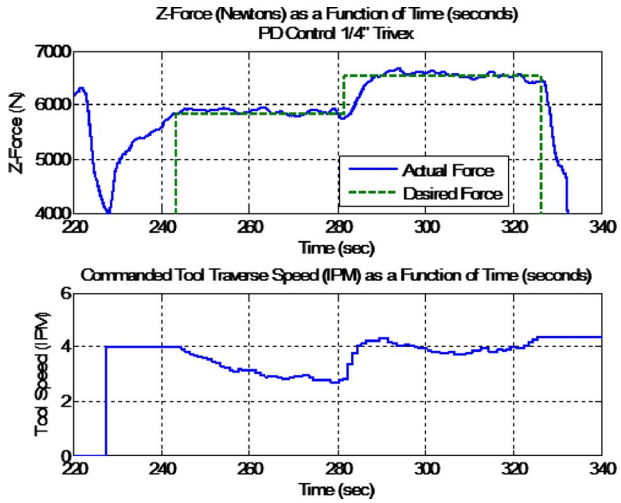

Fig. 15 Regulation and step input with PD control

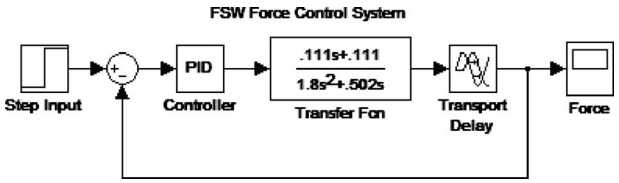

Fig. 16 Simulink model of the FSW force control system

system under P controller differs from PID control. Most notable is the reduction in force overshoot, as evident in Fig. 13. Without the integral action in the controller, the error is not summed and applied to the control law. This results in a much better response to the step input. However, the system's response with P control to a step input resulted in a very small oscillation. The presence of oscillations means the closed loop response of the system under P control exhibits higher order characteristics.

In addition, without the integral action, a notable error exists at the beginning of the weld cycle. This is due to the naturally increasing force as the tool moves into a stiffer work piece environment. Without integral control, the controller is slower to respond to the force disturbance. However, as can be seen, a steady state error does not exist. A steady state error does not emerge because the VFD has an integrator in its controller, and thus produces a tool speed change in response to a force error signal.

The PI control proved to be viable for controlling the welding process as well. A typical result is shown in Fig. 14. The integral term in the controller is evident by two features. The first feature is the relatively large overshoot in response to the 700 N step input. As the integrator summed the error in response to the step, its value was maintained well past the initial rise time.

The second noticeable feature of the system under PI control is the lack of steady state error. At the time the force controller was engaged, the force was naturally rising. The system under PI control responded to this error slightly faster than under P control. However, due to the integral term, an overcorrection in force occurred. Similar to the step response, the oscillation dies out and stability is maintained.

When PD control is applied, excellent control results. Figure 15 shows the systems response to regulation and a step input while under PD control. The derivative term in the control law anticipates force overshoot and implements a correction before the overshoot occurs. As evident in Fig. 15, the systems closed loop response to a step input exhibits first order characteristics. When compared with other controllers previously presented, the PD controller tends to provide a more stable and smooth response.

3.2 Dynamic Model. As previously stated, the system's dynamics are unknown with the exception of the controller. Using the results from the P, PI, PD, and PID version of the controller, it is possible to model the dynamics of the system in response to the step input. Since the results are the responses of the closed loop system, the challenge is to determine the feed forward (or plant) transfer function of the system.

From the results presented in Figs. 12–15, it can be observed how each of the control variations changes the closed loop response. From a mathematical standpoint, the P control architecture alters the feed forward transfer function the least. It simply increases the magnitude of the numerator. Upon review of the closed response to P control, the system tends to behave as a second order system. Assuming the system is an ideal second order system, its closed loop response will take the form shown in Eq. (2). In Eq. (2), ω_n is the system's natural frequency, ζ is the system's damping ratio, and s is the complex variable. From the closed loop equation, the feed forward equation $G_{ol}(s)$ is derived to be of the form listed in Eq. (3). The control diagram shown in Fig. 4 illustrates the systems and the unknowns that had to be determined

$$G_{cl}(s) = \omega_n^2/(s^2 + 2\zeta\omega_n s + \omega_n^2) \tag{2}$$

$$G_{ol}(s) = \omega_n^2/(s(s + 2\zeta\omega_n)) \tag{3}$$

From the results shown in Fig. 12, the amount of overshoot, peak time, and rise time were measured. With these two measurements and treating the response as an ideal second order system, estimates can be made for the natural frequency, damped frequency, and damping coefficients. In addition, the step input of 700 N had to be treated as a unit step in order to obtain the proper value for the overshoot. Thus, the value of overshoot shown in Fig. 12 was normalized in order to obtain an equivalent overshoot in response to a unit step. With the calculated transfer function's coefficients, a Simulink model was constructed to validate the accuracy of the model. The Simulink model was constructed with two feed forward transfer functions. One of the transfer functions was for the known force controller, and the other for the estimated portion of the system.

To fully validate the system, the controller was changed to PID, PI, and PD for the various tests in order to compare with the experimentally obtained results. Since the estimated feed forward transfer was based upon an ideal second order system, initially, only the P control system fit the model. To match the other control architectures, the transfer function had to have the addition of a zero, thus increasing the order of the system. With the addition of the zero, the coefficients of the transfer function were readjusted by best fitting techniques. The completed Simulink model of the system is shown in Fig. 16. The transient response of the system, not including the PID controller, was model by the transfer function given in Eq. (4). In Eq. (4), $F(s)$ is the output force and $R(s)$ is the reference input force

$$F(s)/R(s) = ((0.111s + 0.111)/(1.8s^2 + 0.502))e^{-s} \tag{4}$$

The results of the model are shown on Fig. 17. In each of the tests, a comparison was made to the experimentally obtained results. The model provided results that correlated well with the experimentally obtained results for all the control variations, as can be seen through visual inspection. If desired, the modeled transfer function could now be used to create a nonlinear control architecture that possibly could provide enhanced control.

3.3 Weld Quality. As a validation of the force control architecture to produce good welds, macrosectioning and tensile testing of welds were performed. As with any manufacturing process, validating the ability of the system to produce a good product is essential. Thus, these tests were performed to see if the changing of the traverse speed during the weld cycle affected the quality of

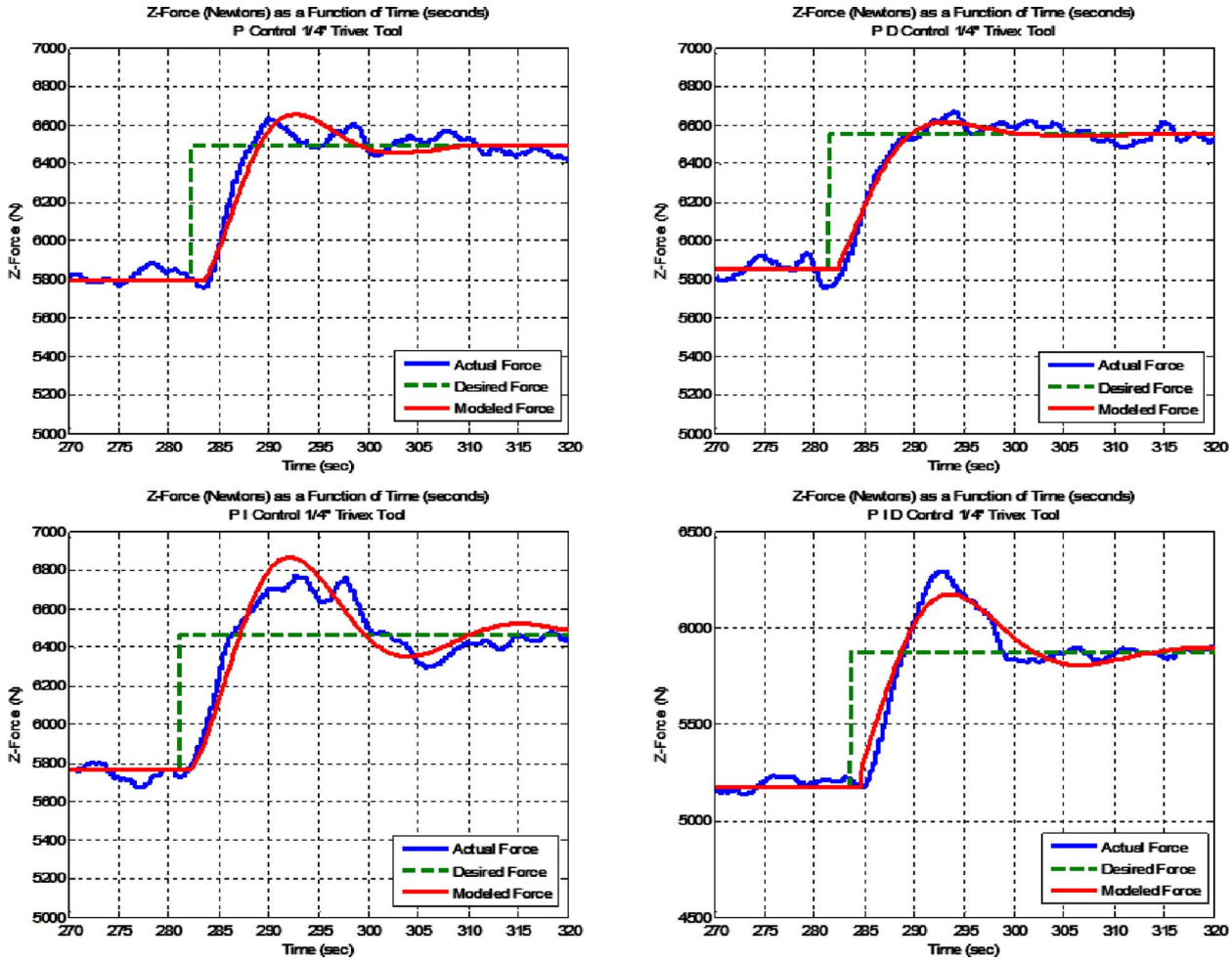

Fig. 17 Results of the modeled transient response of the FSW force control system

the welds in a negative manner.

Figures 18 and 19 are the etched macrosections of two different welds subjected to step inputs. The weld cross section shown in Fig. 18 was produced using the 1/4 in. (6.35 mm) Trivex tool, while the weld shown in Fig. 19 was produced using the 1/4 in. (6.35 mm) threaded tool.

As can be seen in the figures, no evidence of worm holes or internal voids were seen in the cross sections. All welds were found to be acceptable. From the cross sections, the weld nuggets are clearly visible due to their refined grain structures. In comparison to the unaffected parent metal, the weld nuggets grain structure appears to be more refined. This is further evidenced by the small internal voids that are present in the unaffected parent metal. These small voids in the unaffected parent metal and can been seen near the right edge of Figs. 18 and 19.

Fig. 18 Weld using 1/4 in. Trivex tool and force control via traverse speed

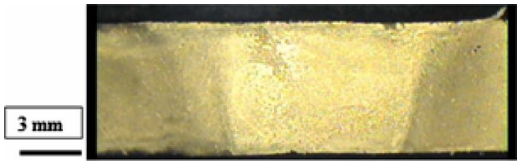

Fig. 19 Weld using 1/4 in. threaded tool and force control via traverse speed

Although acceptable, both welds had a small amount of weld flash deposited on the retreating side of the weld surface. Since the vertical position of the tool is fixed, a robust plunge depth must be set in order to insure the shoulder of the tool remains in contact with the parent metal. As with any stock material, there are variations in the materials dimensions. This was the case in this experiment as well. The plunge depth of the trailing edge of the shoulder was set at 0.001 in. (0.0254 mm). Although a small amount of flash was generated, no surface gouging or negative effects were found in the welds.

Upon closer examination of the weld nuggets, more stirring is evident with the threaded tool than with the Trivex. The threads were designed to push metal down into the lower region of the weld nuggets and help prevent internal voids from forming in this region. When comparing the results in Figs. 18 and 19, the weld nugget for the threaded tool is wider and appears to have been stirred more. Furthermore, a small root flaw is just beginning to form at the bottom surface of the weld produced with the Trivex tool. This root flaw is further evidence of reducing stirring in this region.

Tensile tests were performed to evaluate the strength of the

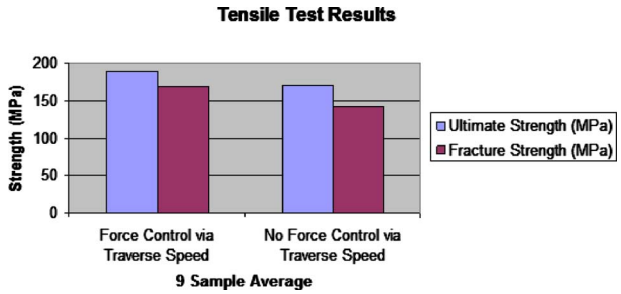

Fig. 20 Tensile test data

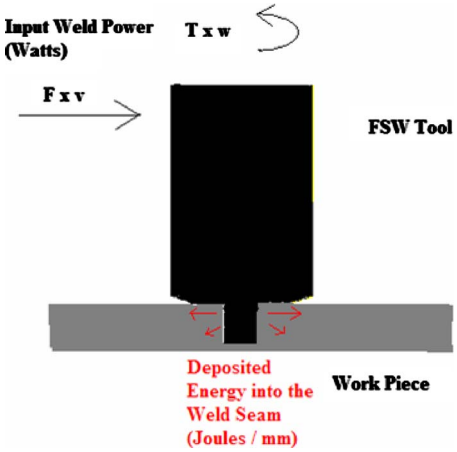

Fig. 21 Energy model

weld. The data in Fig. 20 consists of nine test samples from three weld seams that were created using the Trivex tool. The average ultimate tensile strength of the weld samples was 188 MPa with an average deviation of 8.5 MPa. Thus, the consistency and strength of the welds provides further evidence that the force control method produces welds of acceptable quality. The rather small deviations in tensile strength along with the examined cross sections tend to indicate that worm holes and other material voids are not present.

3.4 Weld Seam Energy Modulation. Another interesting observation is how the axial force correlates with the relative thermal energy beneath the tool since there is not any tool plunge depth change other than what is caused by thermal expansion. In essence, the axial force is an excellent indicator of thermal energy in the welding environment. Although the axial force cannot yet be used to obtain an accurate reading of thermal energy, it can provide information on the relative thermal energy as the weld process proceeds. This can be seen in the base line weld shown in Fig. 7. As the tool moved away from its plunge point where a lot of heating occurred, it entered into a colder region within the work piece. When this occurred, the axial force increased.

With the axial force control of FSW, a constant thermomechanical welding environment is trying to be maintained by the controller. Sinclair [11] showed a correlation between axial force and work piece temperature through preheating experimentation. As the temperature in the welding environment increases, the axial force is reduced. Hence, it can be concluded that not only does the force controller produce a desired force, but it also tries to maintain constant thermomechanical conditions directly beneath the tool. With force control via traverse speed, the energy deposited into the weld seam is modulated to maintain a constant force.

This hypothesis of weld seam energy modulation can be supported with results from Schmidt and Hattel [12], in which they described a thermal model of FSW. They presented Eq. (5), describing the total heat generation Q_{total}

$$\begin{aligned} Q_{\text{total}} &= \delta Q_{\text{sticking}} + (1-\delta) Q_{\text{sliding}} \\ &= 2/3\,\pi\omega[\delta\tau_{\text{yield}} + (1-\delta)\mu p] \\ &\quad \times [(R^3_{\text{shoulder}} - R^3_{\text{probe}})(1-\tan\alpha) \\ &\quad + R^3_{\text{probe}} + 3R^2_{\text{probe}} H_{\text{probe}}] \end{aligned} \tag{5}$$

In this equation by Schmidt and Hattel, the variable δ is the contact state variable or dimensionless slip rate, τ_{yield} is the yield stress of the work piece material at the welding temperature, μ is the coefficient of friction, p is the contact interface pressure, ω is the angular rotation velocity, α is the cone angle of the tool's pin, R_{shoulder} is the shoulder radius of the tool, R_{probe} is the radius of the tool's pin, and lastly, H_{probe} is the height of the tool's pin. Schmidt and Hattel go on to note that the typical expression for a numerical model is in the form of a position dependent surface flux q_{total}. The units of the model take the form of power per unit area. In its final form, the heat generation model can be expressed as Eq. (6), which is a radius dependant surface flux. The simplified equation assumes tool geometry of only a flat shoulder

$$q_{\text{total}} = (3Q_{\text{total}} r)/(2\pi R^3_{\text{shoulder}}) \tag{6}$$

For the hypothesis of weld seam energy modulation to be true, q_{total} must be constant throughout the force controlled welding process. Upon review of the variables in Eqs. (5) and (6), it can be hypothesized that they all become constant when force control via traverse speed is employed and a few assumptions regarding force control are taken into account. First, the plunge depth is constant and does not change as the tool traverses the work piece. Second, the work piece material properties and thickness is constant throughout. Third, a constant axial force produces a constant contact pressure at the interface. Fourth, a constant axial force and a constant plunge depth lead to the other forces acting at the interface, such as torque and traverse force, to be constant as well. Fifth, the constant axial force and torque results in a constant slip rate.

With all of these variables being constant due to force control, a constant rate of heat generation should exist. Notice that the rate of heat generation is not a function of traverse rate. Thus, as the tool traverses along the weld seam at varying speeds, the rate of heat generation is assumed to be the same at any speed. With the force controller varying the traverse speed, a variable amount of energy is deposited per unit length along the weld seam. The intelligence of the control system senses the force beneath the tool and then modulates the amount of energy being deposited into the weld seam directly beneath the tool. By doing this, the controller maintains a constant thermomechanical welding environment.

Using collected process data from the welding experiments, constant heat flux or welding power from the tool can be verified. The simple energy model shown in Fig. 21 uses the forces acting on the tool along with the process parameters of rotation speed and traverse sped to predict the input welding power. Equation (7) predicts the amount of Watts of input weld power. Most of this power is released as heat through both plastic deformation and friction within the welding environment. Using force and process data collected during the welding operation, and after applying it to Eq. (7), a nearly constant input weld power is confirmed in Fig. 22. This confirmation adds validity to the hypothesis that a constant heat flux is present.

The resulting product of torque and tool rotation speed is the primary contributor to the input weld power. The relatively low tool speed and traverse force provide minor contributions to the input weld power, and thus accounts for minor variations of power. To complete the model, Eq. (8) is applied to examine how the changing traverse speed affects the energy deposited into the

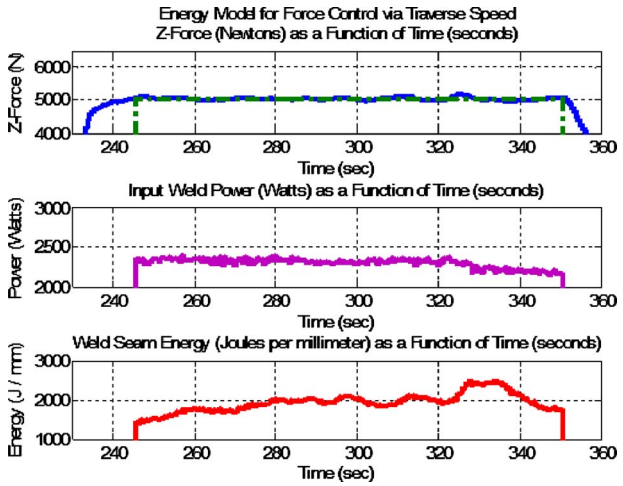

Fig. 22 Results of the energy model

weld seam. As can be seen in Fig. 22, as the tool speed is varied to maintain a constant force, the weld power deposited into the weld environment is modulated.

$$P = (F_t \times v_t) + (T \times \omega) \quad \text{(W)} \tag{7}$$

$$E = P/v_t \quad \text{(J/mm)} \tag{8}$$

Sinclair [11] used this force control architecture to analyze the resulting steady state traverse speed when the work piece was preheated to a desired temperature. His results are shown in Fig. 23. Under the force control algorithm, the FSW tool traversed faster when higher preheating temperatures were used.

For his experiments, Sinclair used a 1/4 in. (6.35 mm) Trivex tool and set the desired axial force at 4000 N. As the work piece was preheated to an elevated temperature, there was less need for process generated heat to soften the work piece. Even though the tool was generating heat at a constant rate, it was being distributed in a manner inversely proportional to the traverse rate. As the preheat temperature was increased for each test, the resulting tool traverse speed increased, since less generated heat was needed beneath the tool. These results support the hypothesis that weld seam energy modulation is obtained as a byproduct when force control is utilized with traverse speed as the controlling variable.

4 Conclusions

Based upon these presented results, it can be concluded that using traverse speed instead of plunge depth as the controlling variable provides much greater accuracy in maintaining a desired axial force. There are two key enablers for obtaining this accuracy. The first enabler is the unidirectional dynamics of the drive motor. The traverse motor never has to reverse its direction. It just simply changes speed. Without having to stop and reverse itself, greater bandwidth and response times are achieved as compared with a motor controlling the plunge depth. The second enabler is load dynamics. The traverse axis of the machine does not support the axial load, thus, the drive system is not burdened by being subjected to the changing load it is trying to control. Although the traverse force does trend with the axial force, its magnitude is substantially less. The drive motor and its VFD are free of the large dynamic forces. When compared with the axial drive system, the axial motor has to stop its motion and change its direction frequently. It is also taxed with the dynamic loading. These two items lead to lower bandwidth and reaction times. In addition, the drive system must be able to support the larger axial load, which requires either greater gear reduction, or a larger drive motor; either of which contribute to the disadvantage of using plunge depth as the controlling variable.

The conclusion that axial force control via traverse speed is better depends upon the equipment being used and the process setup. The welding experiments conducted at Vanderbilt University were conducted on a three axis milling machine. Each axis was controlled independently and aligned with a Cartesian reference frame. Due to a constant plunge depth, the worktable was fixed along the vertical axis during the welding operation. Table movement was only needed along the traverse axis while the force controller was active. In addition, the force control loop resided outside the position control loop. The same results might not be achieved using certain types of robots. For instance, if a six axis jointed-arm robot is to control axial force via traverse speed, more than one linkage must be adjusted simultaneously as the tool continuously traverses along the weld seam. Any simultaneous multilinkage adjustment possibly could result in small fluctuations in the plunge depth of the tool. This will further lead to fluctuations in the axial force and possibly negating the advantages of using traverse speed as the controlling variable. For force control via traverse speed to be successful, there cannot be any linkage adjustment perpendicular to the weld seam. In summary, the vertical position of the tool cannot change relative to the position of the work piece surface. The robot must be capable of maintaining

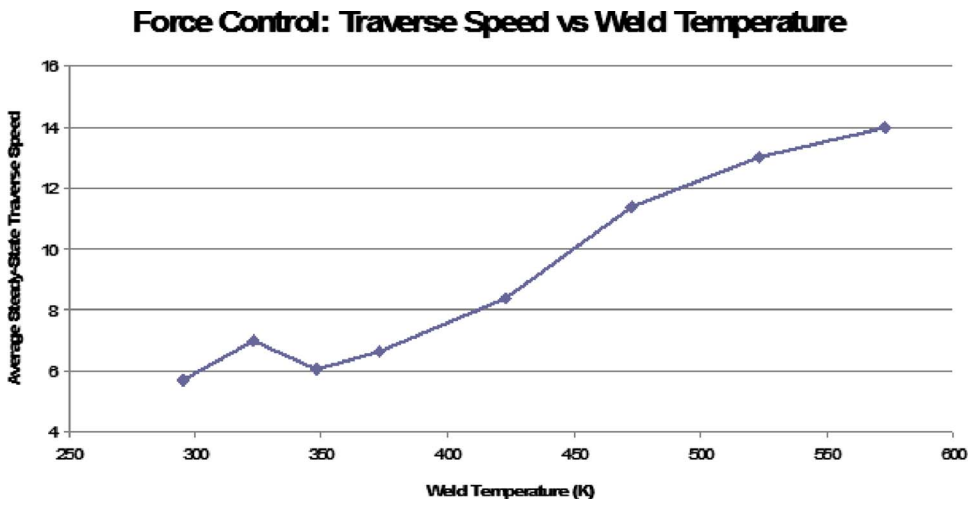

Fig. 23 FSW preheating experiments under force control [11]

noncompliance along the vertical axis of the FSW tool. This force control method probably would work best when the robot's linkages to be adjusted reside in a parallel plane to the weld seam. The linkages could be adjusted via either prismatic or revolute joints. Thus, a selectively compliant assembly robot arm (SCARA), a Cartesian robot or a gantry style machine tool, would be a good candidate for supporting force control via traverse speed. Of course, this is valid provided that the robot or machine is capable of the supporting the high loads associated with FSW. Based upon the results obtained from this experimentation and the load capacities of existing robots, robotic FSW would be restricted to welds less than 1/4 in. (25.4 mm).

The process setup also requires the condition of the welding surface to be relatively constant. With the controlling variable of traverse speed, there is not any means to adjust the vertical position of the tool to changing surface conditions. This requires the plunge depth of the tool to be set to a position, such that the shoulder of the tool will always be in contact with the material. Essentially, the plunge depth must be set as if the welding was being conducted under position control.

Upon further review of the experimentally obtained results, it is interesting to note how the traverse speed of the tool is continuously adjusted to maintain the desired force. It can clearly be seen that the axial force increases as the tool traverses at a faster rate, and decreases as the tool traverses at a slower rate. These results are in agreement with the findings of Cook et al. [3]. The presented energy model confirms that constant input weld power is present and that the force controller modulates the weld seam energy to maintain a constant thermomechanical condition in the welding environment.

Future work can be done to better understand the weld seam energy modulation. How accurately is the welding energy being maintained? This is a major question yet to be answered regarding the hypothesis of weld seam energy modulation. With force control and weld seam energy modulation of FSW, optimum process condition would result that could maximize the strength of the weld. This means that the intelligence of the controller working in conjunction with the machinery, not only would produce a quality weld, but would also produce it with the most efficient speed. The system would naturally insure that adequate heating and force are present in the welding environment beneath the tool.

Along with the investigation of weld seam energy modulation, further modeling work can be done to breakdown the presented transfer function into process and equipment components. The feed forward transfer function models the traverse drive system and the welding process. With this model refinement, more insight would be gained about the welding process itself. In addition, more advanced control algorithms could be developed for force control.

Nomenclature

$F(s)$ = output force
$G_{cl}(s)$ = closed loop response transfer function
$G_{ol}(s)$ = open loop feed forward transfer function
$R(s)$ = input force
E = weld seam energy
F_t = traverse force
K_p = proportional gain
K_i = integral gain
K_d = derivative gain
P = power
$Q_{sliding}$ = heat generation from sliding
$Q_{sticking}$ = heat generation from sticking
Q_{total} = total heat generation
R_{probe} = radius of the probe
$R_{shoulder}$ = radius of the shoulder
T = torque
e = force error
mm = millimeters
p = contact interface pressure
q_{total} = heat flux
r = radius
s = complex variable
t = time
u = control signal
v_t = traverse velocity
α = cone angle of the pin
δ = dimensionless slip rate
π = pi
μ = coefficient of friction
τ_{yield} = yield stress
ω = angular rotation velocity
ω_n = natural frequency
ζ = damping ration

References

[1] Wikipedia, 2009, http://en.wikipedia.org/wiki/Friction_stir_welding
[2] Cook, G., Smartt, H., Mitchell, J., Strauss, A., and Crawford, R., 2003, "Controlling Robotic Friction Stir Welding," Weld. J. (Miami, FL, U.S.), **82**, pp. 28–34.
[3] Cook, G., Crawford, R., Clark, D., and Strauss, A., 2004, "Robotic Friction Stir Welding," Ind. Robot, **31**(1), pp. 55–63.
[4] Smith, C., 2000, "Robotic Friction Stir Welding Using a Standard Industrial Robot," Proceedings of the Second Friction Stir Welding International Symposium, Gothenburg, Sweden.
[5] Soron, M., and Kalaykov, I., 2006, "A Robot Prototype for Friction Stir Welding," Proceedings of the Robotics, Automation and Mechatronics, 2006 IEEE Conference, pp. 1–5.
[6] Zhao, X., Kalya, P., Landers, R., and Krishnamurthy, K., 2007, "Design and Implementation of a Nonlinear Axial Force Controller for Friction Stir Welding Processes," Proceedings of the 2007 American Control Conference, pp. 5553–5558.
[7] Talwar, R., Bolser, D., Lederich, R., and Baumann, J., 2000, "Friction Stir Welding of Airframe Structures," Proceedings of the Second Friction Stir Welding International Symposium, Gothenburg, Sweden.
[8] Strombeck, A., Shilling, C., and Santos, J., 2000, "Robotic Friction Stir Welding—Tool Technology and Applications," Proceedings of the Second Friction Stir Welding International Symposium, Gothenburg, Sweden.
[9] Craig, J., 2005, *Introduction to Robotics Mechanics and Control*, 3rd ed., Prentice-Hall, Englewood Cliffs, NJ.
[10] Ogata, K., 2002, *Linear Control Theory*, 4th ed., Prentice-Hall, Englewood Cliffs, NJ.
[11] Sinclair, P., 2009, "Heated Friction Stir Welding: An Investigation Into How Preheating Aluminum 6061 Affects Process Forces," MS thesis, Vanderbilt University, Nashville, TN.
[12] Schmidt, H., and Hattel, J., 2008, "Thermal Modeling of Friction Stir Welding," Scr. Mater., **58**, pp. 332–337.